CHEMISTRY OF MATERIALS

ARTICLE

pubs.acs.org/cm

Self-Organized Core−Shell Structure for High-Power Electrode in Solid-State Lithium Batteries

Xiaoxiong Xu,[†,‡] Kazunori Takada,[*,†,‡,¶] Ken Watanabe,[§] Isao Sakaguchi,[‡,∥] Kosho Akatsuka,[†,‡,¶] Bui T. Hang,[†,⊥] Tsuyoshi Ohnishi,[†,‡,¶] and Takayoshi Sasaki[†,‡,¶]

[†]International Center for Materials Nanoarchitectonics, National Institute for Materials Science, 1-1 Namiki, Tsukuba, Ibaraki 305-0044, Japan

[‡]NIMS-TOYOTA Materials Center of Excellence for Sustainable Mobility, National Institute for Materials Science, 1-1 Namiki, Tsukuba, Ibaraki 305-0044, Japan

[§]Sensor Materials Center, National Institute for Materials Science, 1-1 Namiki, Tsukuba, Ibaraki 305-0044, Japan

[∥]Optronic Materials Center, National Institute for Materials Science, 1-1 Namiki, Tsukuba, Ibaraki 305-0044, Japan

[¶]Core Research for Evolutional Science and Technology, Japan Science and Technology Agency, 4-1-8, Honcho, Kawaguchi, Saitama 332-0012, Japan

ABSTRACT: Effect of Al-substitution for Co on the electrode properties of $LiCoO_2$ is investigated in a sulfide solid electrolyte. The substitution decreases the electrode resistance and thus improves the high-rate capability. Investigation of the post-annealing effect revealed that, although the crystal structure or morphology of the $LiAl_xCo_{1-x}O_2$ are not significantly changed by the post-annealing, the electrode properties are highly dependent on the post-annealing conditions, which suggests that the improvement in high-rate capability comes from the change in surface structure of the $LiAl_xCo_{1-x}O_2$ particles (i.e., self-organized core−shell structure). The Al-substituted $LiCoO_2$ obtained through this study delivers a discharge capacity of 115 mAh g^{-1} at 1 C and 84 mAh g^{-1} even at a high discharge rate of 5 C at 25 °C, which is one of the highest rate capabilities observed in solid-state cells.

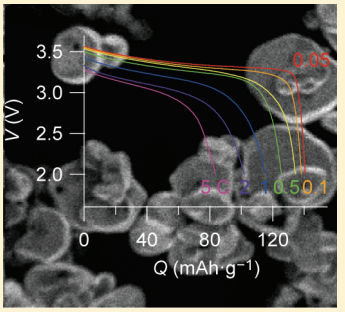

KEYWORDS: lithium battery, solid electrolyte, nanoionics, interface, $LiCoO_2$

INTRODUCTION

Although lithium-ion batteries have been on the market for ~20 years, they are still the subject of much research. One example is the development of solid-state lithium batteries using solid electrolytes, in response to safety issues arising from the combustibility of nonaqueous electrolytes. Nonflammable inorganic solid electrolytes will radically resolve this issue, which is becoming increasingly serious as much larger batteries are now required for electric and hybrid electric vehicles.[1] Although solid-state batteries have suffered from low power density, this is gradually being improved through the development of highly conductive solid electrolytes.[2] In combination with a novel interfacial design between the electrode and the electrolyte to reduce electrode resistance,[3] the power density of solid-state batteries with sulfide solid electrolytes is now comparable to that of commercial lithium-ion cells.

Nevertheless, solid-state lithium batteries are in the pioneering stage, with new frontiers yet to be explored. For example, substitution effects in the cathode materials have been investigated in liquid electrolyte systems. Cathode materials in lithium-ion batteries are generally transition-metal oxides such as $LiCoO_2$, $LiNiO_2$, and $LiMn_2O_4$, and the partial substitution of the transition-metal elements has been reported to influence the electrode performance.[4] However, such substitution effects have rarely been investigated in solid systems; cathode materials studied in solid systems have been simple lithium transition-metal oxides, including $LiCoO_2$. In this study, we substituted part of the Co in $LiCoO_2$ with Al, and investigated the effect on the electrode properties in a sulfide solid electrolyte.

EXPERIMENTAL SECTION

Sample Preparation. $LiAl_xCo_{1-x}O_2$ (x = 0.00−0.25) was prepared from Li_2CO_3, Co_3O_4, and $Al(OH)_3$ (all 99.5% purity, purchased from Wako). The starting materials were weighed at an appropriate ratio and mixed in ethanol by ball milling for 4 h, and then dried at 80 °C for several hours. The mixture was heated at 650 °C for 10 h in air. The precalcined mixture was then pressed into pellets (16 mm in diameter and ~3 mm in thickness) and then calcined at 750 °C for 20 h in air, followed by quenching to room temperature. A planetary ball mill (P-7, Fritsch) was used to regrind the as-sintered samples into powders at 200 rpm for 20 h in ethanol. Finally, the as-ground powder was annealed at 700 °C for 4 h in air in order to remove possible damage caused by the high-energy ball milling.

Sample characterization. The crystal structure of the samples was investigated via powder XRD performed on a Rigaku Rint-2000S powder diffractometer, using graphite-monochromatized Cu Kα radiation. The lattice constants were refined by the least-squares method, using the APPLEMAN program.[5] The microstructure of the samples

Received: December 23, 2010
Revised: July 13, 2011
Published: August 03, 2011

was investigated by scanning electron microscopy (SEM), using a KEYENCE Model VE-8800 microscope. The distribution of Al in the particles was investigated using a secondary-ion mass spectrometer (SIMS) with high lateral resolution (NanoSIMS-50, Cameca). After the surface of the particles was ion-etched to remove contamination, $^{133}Cs^+$ accelerated at 8 keV was tuned on the sample surface, and $(^{27}Al^{16}O)^-$ and $(^{59}Co^{16}O)^-$ molecular ions were collected using a multicollection system to take scanning ion images for Al and Co, respectively. Depth profiles for $(^{27}Al^{16}O)^-$, $(^{59}Co^{16}O)^-$, $(^{7}Li^{16}O)^-$, and ^{28}Si, which comes from the sample holder, were also obtained from the scanning area of 0.8 μm × 0.8 μm until the primary ion beam penetrated the particle.

Electrochemical Measurements. Solid-state electrochemical cells to investigate the electrochemical performance of $LiAl_xCo_{1-x}O_2$ were fabricated using $Li_{3.25}Ge_{0.25}P_{0.75}S_4$ (*thio*-LISICON)[2a] as the solid electrolyte and In−Li alloy as the counter electrode. The working electrode was a mixture of $LiAl_xCo_{1-x}O_2$ and *thio*-LISICON at a weight ratio of 7:3. The working electrode mixture (10 mg), ground electrolyte powder (150 mg), and In−Li alloy formed by attaching a small piece of lithium foil (<1 mg) to indium foil (ca. 60 mg), were pressed together at 500 MPa into a three-layer pellet with 1 cm in diameter. The electrochemical cells were charged and discharged in galvanostatic mode at room temperature using a multichannel galvanostat (PS-08, Toho Giken). The cutoff voltage was set to be 3.58 V for charging and 2.0 V for discharging in order to charge the $LiAl_xCo_{1-x}O_2$ up to 4.2 V vs Li^+/Li, because electrode potential of In−Li alloy counter electrode is 0.62 V vs Li^+/Li. The charging current was fixed at 0.05 C, and discharge current varied between 0.05 and 5 C. In this experiment, 1 C was defined as 137 mA g^{-1} corresponding to 0.5 e^- reaction per hour in $LiAl_xCo_{1-x}O_2$, and was 1.2 mA cm^{-2} in current density. After the cells were charged to 3.58 V for the second time, the electrode impedance was measured by electrochemical impedance spectroscopy (EIS), using a frequency response analyzer (VSP, Bio-Logic SA). The AC perturbation signal was 10 mV, and the frequency range was from 4 × 10^5 to 1 × 10^{-2} Hz.

RESULTS AND DISCUSSION

Effect of the Al-substitution on the Electrode Properties of $LiCoO_2$. Figure 1a shows the powder X-ray diffraction (XRD) patterns of $LiAl_xCo_{1-x}O_2$, which indicate that the Al substitution did not change the α-$NaFeO_2$-type structure of $LiCoO_2$. All the reflections were indexable on a rhombohedral lattice with a space group of $R\bar{3}m$.[6] The lattice constants were refined based on the rhombohedral lattice and are plotted against the Al content (x in $LiAl_xCo_{1-x}O_2$) in Figure 1b. They changed linearly with x and agreed with the results reported in ref 7, suggesting that the Al is substituted for Co in these samples as well, as revealed in the literature.

Figures 2 and 3 indicate changes in the electrode properties caused by the Al substitution. Each impedance spectrum obtained for the In−Li/$LiAl_xCo_{1-x}O_2$ cell consists of a distorted semicircle with a slope at low frequencies, as shown in Figure 2. The high-frequency intercepts of the semicircles on the real axis are attributable to the resistance of the electrolyte layer, because they were independent of the $LiAl_xCo_{1-x}O_2$ samples and consistent with that expected from the dimensions of the electrolyte layer in the electrochemical cell and the conductivity of the *thio*-LISICON. Impedance of the In−Li counter electrodes was too small to be seen in the plots. Since the semicircles are distorted and asymmetric, the spectra could not be explained by a simple Randles model; however, it is clear that the Al substitution reduced the electrode resistance: the diameter of the semicircles

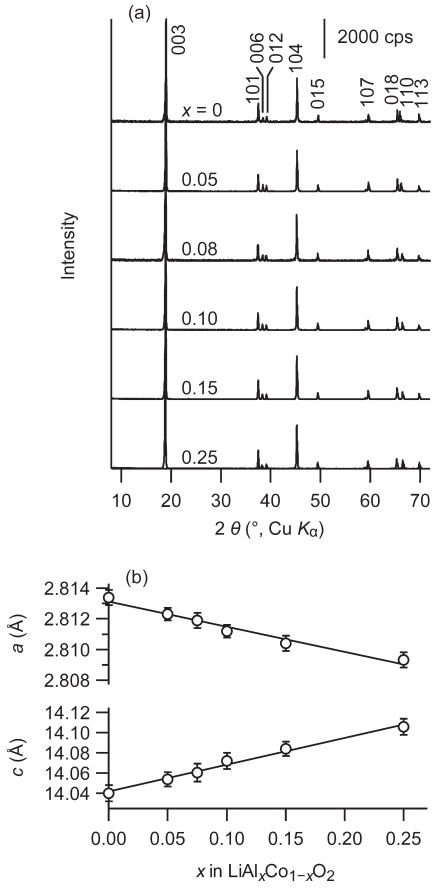

Figure 1. (a) Powder XRD patterns and (b) lattice constants for $LiAl_xCo_{1-x}O_2$ post-annealed at 700 °C for 4 h.

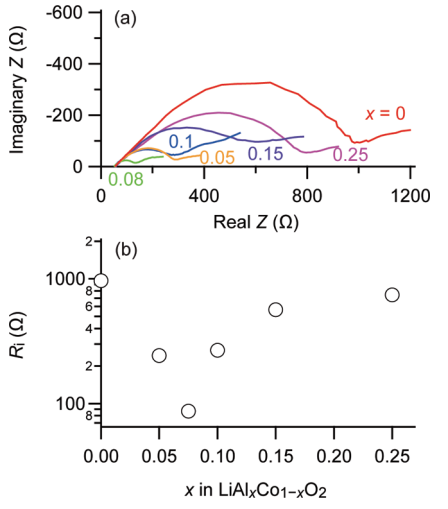

Figure 2. (a) Changes in electrode impedance of $LiAl_xCo_{1-x}O_2$ upon the Al substitution. (b) Diameter of the distorted semicircles (R_i) in the complex impedance plots of the In−Li/$LiAl^xCo_{1-x}O_2$ cells in panel a is plotted against x.

(R_i) decreased from 960 Ω at x = 0 to 87 Ω at x = 0.08, as shown in Figure 2b.

The decreasing R_i indeed improved the rate capability of the $LiCoO_2$ electrode. When the pristine $LiCoO_2$ was discharged at

dx.doi.org/10.1021/cm103665w |*Chem. Mater.* 2011, 23, 3798–3804

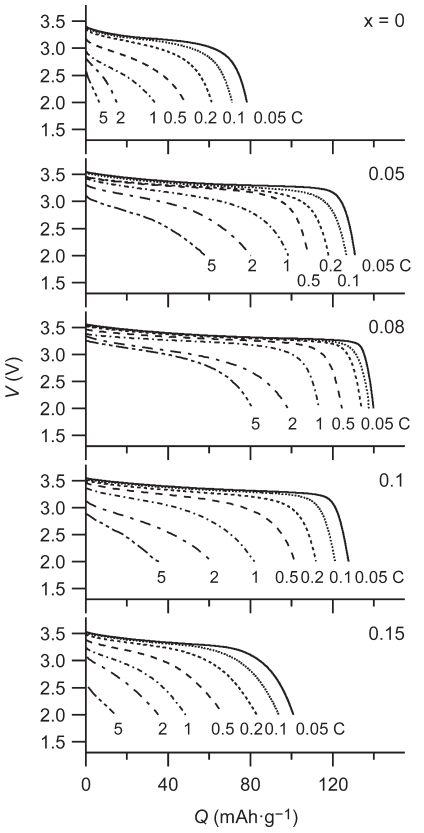

Figure 3. Discharge curves of the In−Li/$LiAl_xCo_{1-x}O_2$ cells at different discharge rates from 0.05 C to 5 C. It should be noted that the electrode potential of the In−Li counter electrode is 0.62 V vs Li^+/Li, and thus 4 V plateaus that $LiAl_xCo_{1-x}O_2$ shows appeared at $V \approx 3.5$ V.

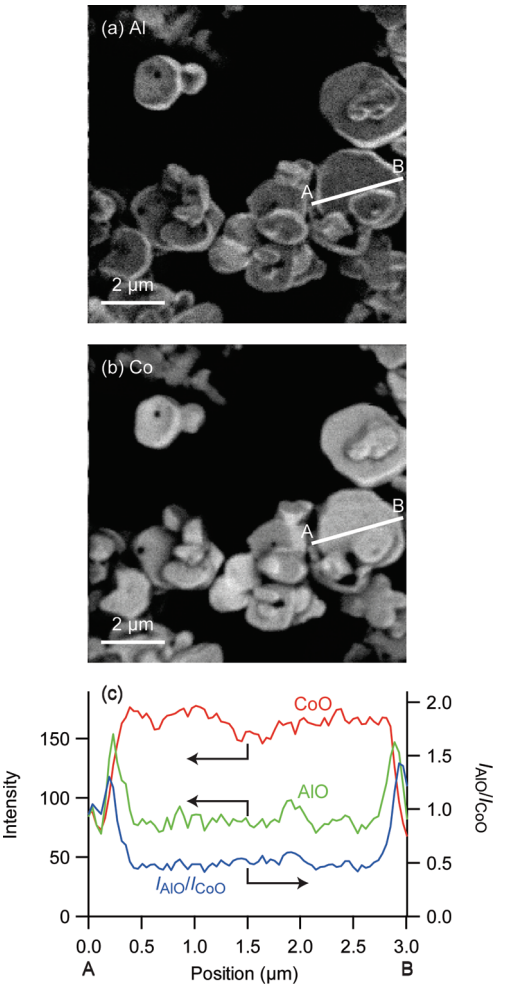

Figure 4. Elemental mapping of $LiAl_{0.08}Co_{0.92}O_2$ particles taken by two-dimensional SIMS: (a) signal intensity for $(^{27}Al^{16}O)^-$ molecular ions; (b) signal intensity for $(^{59}Co^{16}O)^-$ molecular ions; and (c) signal intensity along line A−B shown in panels a and b.

various current densities, it gave only a small discharge capacity at 5 C. The Al substitution improved the rate capability: the capacity at 5 C reached 80 mAh g^{-1} at $x = 0.08$, as shown in Figure 3.

Conceivable Mechanism of the Rate-Capability Enhancement. These results demonstrate that the partial substitution of Al for Co increases the power density of the $LiCoO_2$ cathode in solid-state lithium batteries. The improvement may be attributable to enhanced ionic diffusion in $LiCoO_2$ by the substitution, as reported for liquid electrolyte systems.[8] However, our previous study[3] revealed that the rate-determining step in the electrode reaction of $LiCoO_2$ is in the $LiCoO_2$/electrolyte interface. This suggests that even the enhancement of ionic diffusion by the Al substitution will not increase the power density without the reduction of interfacial resistance.

In the study,[3] the rate-determining factor was considered to be a highly developed space-charge layer on the electrolyte side at the interface, which is generated by the difference in electrochemical potential of Li ions between the $LiCoO_2$ and the sulfide electrolyte, and is developed by electronic conduction in the $LiCoO_2$. Since Li ions are depleted there, it would be high in resistance and thus rate-limiting. In order to suppress the development, we interposed a thin layer of oxide solid electrolyte at the interface as a buffer layer, which drastically increased the power density. There are several similarities between the present results and those obtained in our previous study.

In our previous study, surface of the $LiCoO_2$ particles was covered with oxide solid electrolytes for interposition as a buffer layer between the $LiCoO_2$ and the sulfide solid electrolyte upon contact with the sulfide solid electrolyte. A thin film of oxide solid electrolyte layer was formed on the surface of the $LiCoO_2$ particles by spray coating. When the oxide solid electrolyte was applied to the surface, the electrode resistance began to decrease, because the oxide solid electrolyte layer reduced the interfacial resistance where it was formed. Increasing the amount of applied electrolyte decreased the resistance due to the increasing coverage, i.e., increasing interfacial area where the buffer layer suppressed the development of a space-charge layer. After the resistance reached a minimum, further application of the oxide electrolyte increased the electrode resistance, because the buffer layer became thick enough for its resistance to be rate-determining. Similarly, in this study, the electrode resistance decreased with increasing Al content. It showed a minimum at $x = 0.08$ and then increased with increasing Al content.

In addition, the current drain observed in this study was larger than 6 mA cm^{-2}, which is also in agreement with that observed in our previous study. Since increasing power density is essential for the development of solid-state lithium batteries, numerous attempts have been made to achieve this goal. For example, several conductive additives were introduced for this purpose;[9]

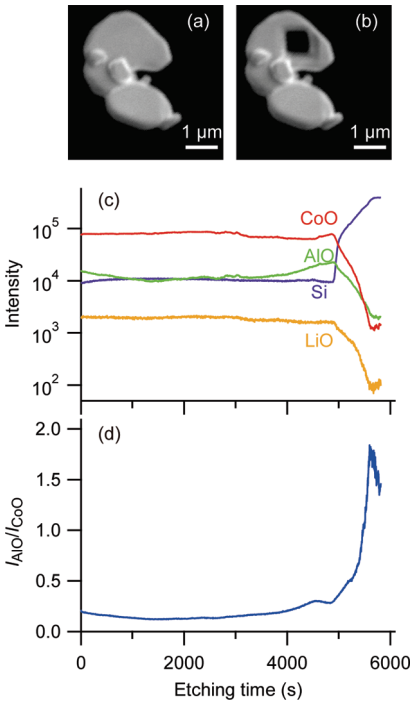

Figure 5. Secondary ^{16}O images of the particle (a) before depth analysis and (b) after depth analysis. Depth profiles for $(^{27}Al^{16}O)^-$, $(^{59}Co^{16}O)^-$, $(^{7}Li^{16}O)^-$, and ^{28}Si also are shown ((c) signal intensities and (d) calculated intensity ratio of I_{AlO}/I_{CoO}).

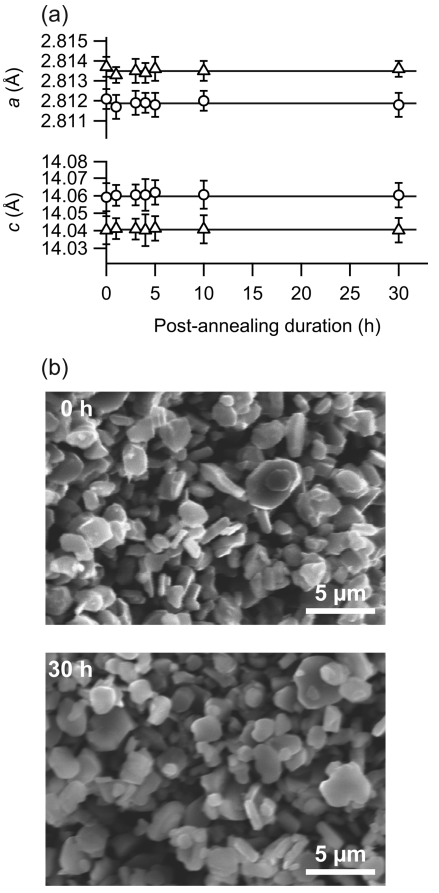

Figure 6. (a) Lattice constants and (b) SEM images of the $LiAl_xCo_{1-x}O_2$ by post-annealing at 700 °C for different durations. In panel a, triangles (△) and circles (○) indicate the lattice constants of the samples with $x = 0$ and 0.08, respectively. SEM images were taken for the sample with $x = 0.08$ before and after post-annealing for 30 h.

however, the current drains were still smaller than the order of 1 mA cm^{-2}. In other words, a large current drain of ~10 mAh cm^{-2} has been reported only when oxide solid electrolytes were interposed between $LiCoO_2$ and the sulfide solid electrolytes. These similarities suggest that the introduction of Al forms a surface layer on the $LiCoO_2$ particles to act as an oxide solid electrolyte. That is, the enhancement of high-rate capability may not come from the Al introduced into the Co site that promotes the ionic diffusion in $LiCoO_2$ but rather from the Al residing on the surface and forming a surface layer, which acts as the buffer layer. A recent study on the crystal structure of $LiAl_xNi_{1-x}O_2$[10] supports this idea.

A study using diffraction techniques combined with elemental analysis revealed that Al and Ni in $LiAl_xNi_{1-x}O_2$ tend to segregate to form Al- and Ni-rich domains, and the segregation induces anisotropic strain in the $Al_xNi_{1-x}O_2$ slabs. A similar segregation may occur in this $LiAl_xCo_{1-x}O_2$ system as well, because they have similar characteristics.[11] If this segregation did occur, it would preferentially form the Al-rich domains at the surface to release the strain.[12] These domains would act as an oxide solid electrolyte layer to reduce the electrode resistance when the $LiAl_xCo_{1-x}O_2$ particles are embedded in the solid-state cell, because the electronic conductivity of the Al-rich domains would be low, because of the low concentration of Co.

In fact, enriched Al was detected in the two-dimensional SIMS images shown in Figure 4. Since the ion-etching preceding the observation removed the front surface of the particles, the images of the center and the edge of the particles show the inner and outer information of the $LiAl_xCo_{1-x}O_2$ particles, respectively. The image taken for $LiAl_{0.08}Co_{0.92}O_2$ (Figure 4a) shows a strong signal for $(^{27}Al^{16}O)^-$ at the edges. In addition, the line profiles of the signal intensities in Figure 4c show that the strong signal for $(^{27}Al^{16}O)^-$ appeared near the edge where that for $(^{59}Co^{16}O)^-$ was weakened.

The distribution of Al in a particle along the vertical direction was also investigated by a depth analysis. The depth profiles in Figure 5c and 5d were taken from the front surface to the back surface until the particle was completely penetrated, as shown in Figures 5a and 5b. Because the front surface was lost during the equipment adjustment, an increase in I_{AlO}/I_{CoO} was not found in the beginning of the profiles. On the other hand, it clearly increased at the end of the profile (i.e., at the back surface of the particle). Because the signal intensities in the middle of the profiles should correspond to the compositions in the bulk, the composition ratio of [Al]/[Co] at the back surface can be roughly estimated from the intensity ratio of I_{AlO}/I_{CoO} at the end of the profile, using the relation between [Al]/[Co] and I_{AlO}/I_{CoO} obtained from the bulk. Because a value of [Al]/[Co] = 0.08/0.92 in the bulk gives a value of $I_{AlO}/I_{CoO} = 0.13$ in the middle of the profile, a value of $I_{AlO}/I_{CoO} = 1.8$ at the back surface will correspond to a value of [Al]/[Co] = 0.53/0.47. These results strongly suggest that Al was enriched at the surface of the particles.

Note that I_{AlO}/I_{CoO} in the center of the line profile in Figure 4c was much larger than that in the middle of the depth profile in Figure 5d, although both were considered to correspond to the bulk composition. A conceivable explanation for

dx.doi.org/10.1021/cm103665w |*Chem. Mater.* 2011, 23, 3798–3804

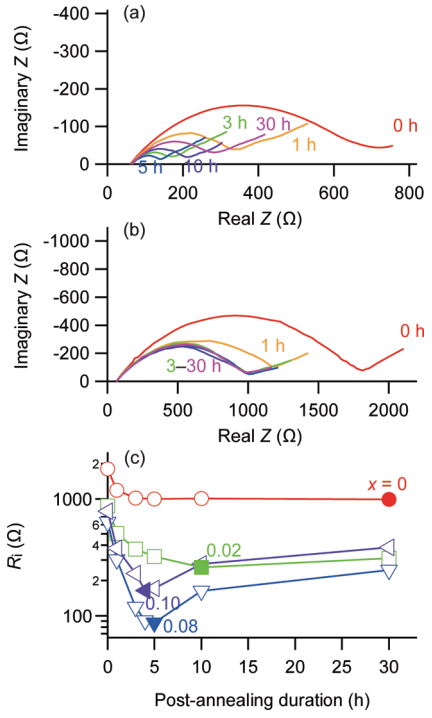

Figure 7. Changes in electrode impedance of $LiAl_xCo_{1-x}O_2$ upon post-annealing. R_i estimated from the complex impedance plots for the $LiAl_xCo_{1-x}O_2$ with (a) $x = 0.08$ and (b) $x = 0$ are plotted with that for the samples with $x = 0.02$ and 0.10 in panel c, as a function of post-annealing duration. The lowest R_i value for each sample is indicated by a solid symbol.

this disagreement is that ion etching before the two-dimensional observation did not completely remove the front surface of the particle. Part of the Al-enriched surface might still remain to increase the I_{AlO}/I_{CoO}, and this may be more evidence of the presence of the Al-enriched domains at the surface.

Effect of Post-Annealing. If the above scenario is true, post-annealing would affect the electrode properties of $LiAl_xCo_{1-x}O_2$. In the above experiments, the synthesized $LiAl_xCo_{1-x}O_2$ was ground once into powder using a planetary ball mill and then post-annealed to remove any damage caused by the milling. The ball milling should give the appearance of fresh surface with the same composition as the bulk, because it is cleaved open from the bulk. In this situation, the post-annealing intended to remove damage will also induce diffusive mass transfer and promote segregation and reconstruction of the surface structure with predominant Al-rich domains. Since they should grow with post-annealing duration, the electrode properties are likely to change with the post-annealing time. In order to verify this hypothesis, we investigated the effect of post-annealing on the electrode properties, where the as-ground powder was post-annealed under relatively moderate conditions of 700 °C, so that the crystal structure and the morphology would remain unchanged.

The post-annealing did not change the crystal structure or morphology, as confirmed by XRD and SEM observation, respectively. The lattice constants refined from the XRD results for the post-annealed samples were constant within the estimated standard deviations, as shown in Figure 6a, indicating that the post-annealing for 30 h did not affect the crystal structure. The post-annealing did not change the particle size either, as shown in Figure 6b. On the other hand, the post-annealing greatly changed the electrode properties of the $LiAl_{0.08}Co_{0.92}O_2$, as demonstrated in Figures 7 and 8.

The post-annealing decreased R_i in the beginning and increased it again after R_i reached a minimum at a post-annealing duration of 5 h, as shown in Figure 7a. The change was predictable from the above discussion. The decreasing R_i in the beginning can be attributable to the formation of Al-rich domains acting as the buffer layer. On the other hand, prolonged post-annealing will allow the Al-rich domains to grow and form thick Al-rich layers. Because lithium aluminum oxides, which are the presumable compounds at the surface, are poor ionic conductors, the resistance of the thick Al-rich layer will become high and dominant in the electrode reaction to increase the R_i value again. In addition, the composition dependence of R_i value was reasonable. When x is smaller, it will need more time to make enough Li ions diffuse to the surface and reduce the R_i value, and vice versa. In fact, $LiAl_xCo_{1-x}O_2$ with $x = 0.02$, 0.08, and 0.10 showed the lowest R_i values at post-annealing durations of 4, 5, and 10 h, respectively, as indicated in Figure 7c.

The above scenario also predicts that the post-annealing will not affect the electrode properties of $LiCoO_2$, because such segregation, or formation, of Al-rich domains would not occur in pristine $LiCoO_2$. In fact, the R_i value was constant after the post-annealing for 3 h, as shown in Figures 7b and 7c. However, the R_i value was decreased from 1.8 kΩ to 1.0 kΩ in the beginning of post-annealing. High-energy ball milling is known to cause damage including formation of oxygen vacancies, especially on the surface,[13] which affects catalytic[14] and electrochemical[15] properties. Since post-annealing will remove the defects, the change in the beginning would be attributable to the removal of the damage.

Removal of the damages would also contribute to the decrease in the R_i value observed for the $LiAl_{0.08}Co_{0.92}O_2$. Although detailed experiments are underway to distinguish between the contributions of the two effects, it seems reasonable to consider that the segregation contributes greatly to the change in the electrode resistance. The defects can be removed only by displacement of the atoms, while the segregation requires transport of the atoms. Therefore, the effect of the segregation should be observed for a longer time. In fact, the electrode resistance changed over 30 h for $LiAl_{0.08}Co_{0.92}O_2$, while a period of only 3 h was required for $LiCoO_2$. In addition, the post-annealing decreased the R_i value from 630 Ω to 120 Ω in the beginning (i.e., to one-fifth for $LiAl_{0.08}Co_{0.92}O_2$, while only to one-half for $LiCoO_2$). These differences strongly suggest that the segregation forming the Al-rich domains predominantly reduces the electrode resistance of $LiAl_{0.08}Co_{0.92}O_2$.

As expected from the changes in electrode resistance, the high-rate capability of $LiAl_{0.08}Co_{0.92}O_2$ changed with the post-annealing time. The $LiAl_{0.08}Co_{0.92}O_2$ post-annealed for 5 h, where the R_i value was minimum, showed the best performance among the samples, which delivered 84 mAh g^{-1} at 5 C discharge, as shown in Figure 8a. The performance was almost comparable to, or higher than, that observed in our previous study, where the surface of $LiCoO_2$ was coated with an oxide solid electrolyte buffer layer such as $Li_4Ti_5O_{12}$ and $LiNbO_3$.

CONCLUSIONS

The effects of Al substitution in $LiCoO_2$ on the electrode properties were investigated in a sulfide solid electrolyte. The

dx.doi.org/10.1021/cm103665w |*Chem. Mater.* 2011, 23, 3798–3804

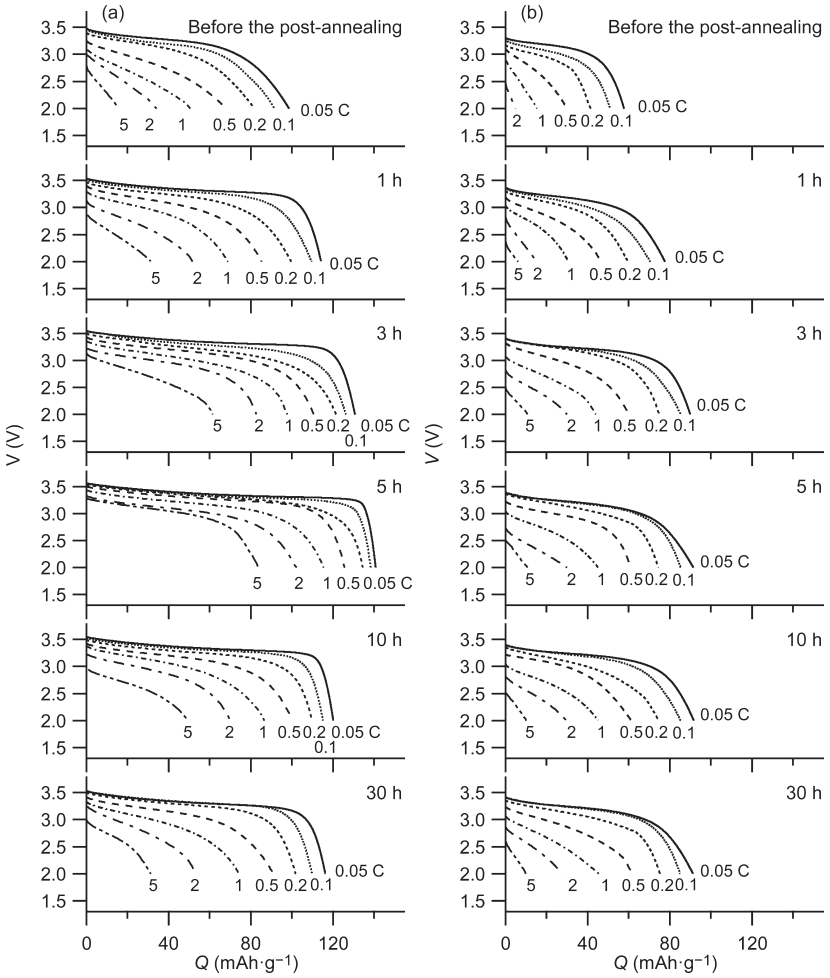

Figure 8. Discharge curves of the $LiAl_xCo_{1-x}O_2$ with (a) $x = 0.08$ and (b) $x = 0$, post-annealed for different durations in In−Li/$LiAl_xCo_{1-x}O_2$ cells.

substitution improved the rate capability to enable the $LiAl_xCo_{1-x}O_2$ to deliver a discharge capacity of 84 mAh g^{-1} at 5 C discharge. The improvement is considered to come from the formation of Al-rich layer on the $LiAl_xCo_{1-x}O_2$ particles, which acts as a buffer layer to reduce the interfacial resistance.

Interfacial phenomena typified by "nanoionics"[16] are attracting a great deal of attention in studies on electrochemical devices, because their importance for the electrode performance is now recognized. Therefore, a great number of studies have examined the surface coating of active materials, as reviewed in ref 17, to control the interfacial phenomena. In such studies, nanometer-thick coating layers were formed on the surface of the active materials; however, the stability of the nanostructure is a concern. Heat treatment or high-temperature operation induces interdiffusion between the active and coating materials, causing a loss of the coating layer.[18] On the other hand, the segregated Al-rich layers in this study grow upon post-annealing. That is, the core−shell structure is self-organized and thus will be much more stable. In addition, a coating process is not necessary, because the layers are formed automatically during the calcination process, although they were formed by post-annealing in this study. Consequently, the Al-substituted $LiCoO_2$ is regarded as more suitable and practical for cathode materials in solid-state lithium batteries, with comparable performance to coated materials.

AUTHOR INFORMATION

Corresponding Author

*Phone: +81-29-860-4317. Fax: +81-29-854-9061. E-mail: takada.kazunori@nims.go.jp.

Present Addresses

⊥International Training Institute for Materials Science, Hanoi University of Technology, 1 Dai Co Viet, Hai Ba Trung, Ha Noi, Vietnam.

ACKNOWLEDGMENT

This work was partly supported by a Grant-in-Aid for Scientific Research on Priority Areas, "Nanoionics 439"; and the "World Premier International Center Initiative (WPI Initiative) on Materials Nanoarchitectonics" and the "MEXT Program for Development of Environmental Technology using Nanotechnology", Ministry of Education, Culture, Sports, Science and Technology (MEXT), Japan.

REFERENCES

(1) Li, W.; Dahn, J. R.; Wainwright, D. S. *Science* **1994**, *264*, 1115.

(2) (a) Kanno, R.; Murayama, M. *J. Electrochem. Soc.* **2001**, *148*, A742. (b) Mizuno, F.; Hayashi, A.; Tadanaga, K.; Tatsumisago, M. *Adv. Mater.* **2005**, *17*, 918.

(3) (a) Ohta, N.; Takada, K.; Zhang, L. Q.; Ma, R. Z.; Osada, M.; Sasaki, T. *Adv. Mater.* **2006**, *18*, 2226. (b) Ohta, N.; Takada, K.; Sakaguchi, I.; Zhang, L. Q.; Ma, R. Z.; Fukuda, K.; Osada, M.; Sasaki, T. *Electrochem. Commun.* **2007**, *9*, 1486.

(4) (a) Tarascon, J. M.; Wang, E.; Shokoohi, F. K.; McKinnon, W. R.; Colson, S. *J. Electrochem. Soc.* **1991**, *138*, 2859. (b) Jones, C. D. W.; Rossen, E.; Dahn, J. R. *Solid State Ionics* **1994**, *68*, 65. (c) Song, D.; Ikuta, H.; Uchida, T.; Wakihara, M. *Solid State Ionics* **1999**, *117*, 151. (d) Koksbang, R.; Barker, J.; Shi, H.; Saïdi, M. Y. *Solid State Ionics* **1996**, *84*, 1.

(5) Appleman, D. E.; Evans, H. T.; Handwerker, D. S. *Program X-ray, Geological Survey*; U.S. Department of the Interior: Washington, DC, 1966.

(6) Johnston, W. D.; Heikes, R. R.; Sestrich, D. *J. Phys. Chem. Solids* **1958**, *7*, 1.

(7) (a) Khan, M. N.; Bashir, J. *Mater. Res. Bull.* **2006**, *41*, 1589. (b) Gaudin, E.; Taulelle, F.; Stoyanova, R.; Zhecheva, E.; Alcántara, R.; Lavela, P.; Tirado, J. L. *J. Phys. Chem. B* **2001**, *105*, 8081. (c) Dahéron, L.; Dedryvére, R.; Martinez, H.; Flahaut, D.; Ménétrier, M.; Delmas, C.; Gonbeau, D. *Chem. Mater.* **2009**, *21*, 5607.

(8) (a) Myung, S.-T.; Kumagai, N.; Komaba, S.; Chung, H.-T. *Solid State Ionics* **2001**, *139*, 47. (b) Castro-García, S.; Castro-Couceiro, A.; Señarís-Rodríguez, M. A.; Soulette, F.; Julien, C. *Solid State Ionics* **2003**, *156*, 15.

(9) (a) Takahara, H.; Takeuchi, T.; Tabuchi, M.; Kageyama, H.; Kobayashi, Y.; Kurisu, Y.; Kondo, S.; Kanno, R. *J. Electrochem. Soc.* **2004**, *151*, A1539. (b) Mizuno, F.; Hayashi, A.; Tadanaga, K.; Tatsumisago, M. *J. Power Sources* **2005**, *146*, 711. (c) Mizuno, F.; Hayashi, A.; Tadanaga, K.; Tatsumisago, M. *J. Electrochem. Soc.* **2005**, *152*, A1499. (d) Mizuno, F.; Hayashi, A.; Tadanaga, K.; Tatsumisago, M. *Solid State Ionics* **2006**, *177*, 2731.

(10) Croguennec, L.; Shao-Horn, Y.; Gloter, A.; Colliex, C.; Guilmard, M.; Fauth, F.; Delmas, C. *Chem. Mater.* **2009**, *21*, 1051.

(11) Guilmard, M.; Pouillerie, C.; Croguennec, L.; Delmas, C. *Solid State Ionics* **2003**, *160*, 39.

(12) Nowotny, J. *Solid State Ionics* **1988**, *28*−*30*, 1235.

(13) (a) Mestl, G.; Verbruggen, N. F. D.; Knözinger, H. *Langmuir* **1995**, *11*, 3035. (b) Hirai, M.; Ikeya, M. *Jpn. J. Appl. Phys.* **2004**, *43*, 5369.

(14) Rougier, A.; Soiron, S.; Haihal, I.; Aymard, L.; Taouk, B.; Tarascon, J.-M. *Powder Technol.* **2002**, *128*, 139.

(15) Amade, R.; Heitjans, P.; Indris, S.; Finger, M.; Haeger, A.; Hesse, D. *J. Photochem. Photobiol. A* **2009**, *207*, 231.

(16) Maier, J. *Prog. Solid State Chem.* **1995**, *23*, 171.

(17) Chen, Z.; Qin, Y.; Amine, K.; Sun, Y.-K. *J. Mater. Chem.* **2010**, *20*, 7606.

(18) Takada, K.; Ohta, N.; Zhang, L. Q.; Fukuda, K.; Sakaguchi, I.; Ma, R. Z.; Osada, M.; Sasaki, T. *Solid State Ionics* **2008**, *179*, 1333.